

UNSUPERVISED COLOR ALIGNMENT FOR CROSS - CAMERA IMAGING APPLICATIONS

Dr.K.Babu Rao, N.Pujitha, A.Madhu, SK.Ayesha sultana, Y.SambaSiva rao

Usha Rama college of engineering and technology

ABSTRACT

Consistent color representation across imaging devices is crucial for numerous scientific applications. However, the inherent variations in image formation processes and the restricted access to native sensor data, particularly in consumer-grade cameras like smart phones, hinder reliable color assessment and impair computer vision performance. To address this challenge, we propose a color alignment framework that treats camera image formation as a black-box system and decomposes the color alignment task into three distinct stages: camera response calibration, response linearization and color matching. Our model can operate with non-standard color references, i.e., color patches with unknown true values, by leveraging a novel "balance-of-linear distances" feature. This approach is equivalent to determining camera parameters through an unsupervised learning process. Moreover, our method requires only a minimal set of corresponding color patches across the images to be aligned, thereby facilitating practical implementation. We evaluated our model's performance on three challenging image datasets, acquired under diverse illumination and exposure conditions by multiple cameras, including one dataset emulating uncommon scenarios encountered in scientific imaging applications. Comprehensive benchmarking demonstrated that our proposed color alignment model outperformed other popular and state-of-the-art methods, underscoring its efficacy and potential for widespread adoption.

Keyword: *patches, benchmarks, nonstandard color references, linearization.*

1. Introduction:

Color constancy refers to the ability to perceive the inherent color of objects independent of the illumination source. It finds applications ranging from colorimetric analysis for comparing scene objects to object recognition tasks and applied to the image to mitigate the effects of scene illumination [4, 5].

However, existing techniques can only establish ground truth colors within camera-specific color spaces, making it challenging to map the same color surface imaged by different cameras to consistent values.

An alternative approach to achieving color constancy involves camera calibration in advance. As per the ISO 17321-1:2012 standard [9], two primary techniques exist: the spectral method and the target method. Extensive research [Epstein, 1977; Walsh & Kulikowski, 1998] has demonstrated that the compensation achieved by our visual system for various constancies depends on the richness of contextual cues available, as elegantly shown in the classic size constancy experiments by Holway and Boring [1941].

Unlike the human visual system, which can inherently reduce the effects of illumination changes to maintain consistent color perception [4], digital cameras lack this ability. Consequently, white balancing techniques are applied to images captured by RGB digital cameras to mitigate color distortions arising from illumination spectra [1, 2, 3, 5].

1.1 Spectral Method

The spectral method measures image sensor's response in a continuous range of wavelength and requires elaborate laboratory equipment. A change in illumination affects the pixel values of an image taken with an RGB digital camera because the values are determined by spectral information such as the spectra of illumination [1,2,3].

1.2 Target Method

The target method calibrates the camera by measuring the color patches on a standard color target, e.g., the Macbeth color chart. Both of these methods require standard color reference and are unpractical for normal end-users. Perceptual constancies are the workhorse of our sensory abilities. In vision, the stimulation on the retina is extremely variable with respect to size, form, speed, and wavelength. Yet, we do perceive a stable world where, for example, an object does not appear to change when we walk past it, even though changes in distance, projection, eccentricity, and illumination might lead to a vastly different stimulation of our visual system.

2. Literature Survey:

Color constancy, the ability to perceive stable surface colors across changes in illumination, has been a topic of extensive research and debate. While some researchers argue that color constancy is severely limited due to issues like metamerism (Logvinenko et al., 2015; Witzel et al., 2016), with empirical studies reporting low levels of compensation around 20% (Arend & Reeves, 1986; Tiplitz et al., 1988; Valberg & Lange-Malecki, 1990), others have found that color constancy can reach levels of about 80% when additional cues are present in the visual stimulus (Kraft & Brainard, 1999). Over time, the degree of experimentally measured color constancy appears to have steadily increased (Foster, 2011; Witzel & Gegenfurtner, 2018).

This controversy may partly stem from the introduction of strict methods to quantify color constancy as a single numerical value. Historically, Many 20th-century studies reporting low constancy levels employed asymmetric matching techniques with different simulated illuminants on a CRT monitor, where observers matched the colors of test objects across illuminated regions (Arend & Reeves, 1986). While allowing for testing arbitrary surface colors, Higher constancy levels around 80% have been observed in paradigms with increased immersion, such as achromatic matching, sequential matching, or color categorization under a single, full-field illuminant (Brainard, 1998; Foster et al., 2001; Hansen et al., 2007; Olkkonen et al., 2009, 2010; Smithson & Zaidi, 2004).

3. PROPOSED METHOD:

As The proposed color alignment framework, as illustrated in Fig., consists of three main steps: camera response calibration, response linearization, and color matching. The camera response calibration estimates the inverse of the nonlinearity in color intensities measured by a camera with respect to the scene radiance.

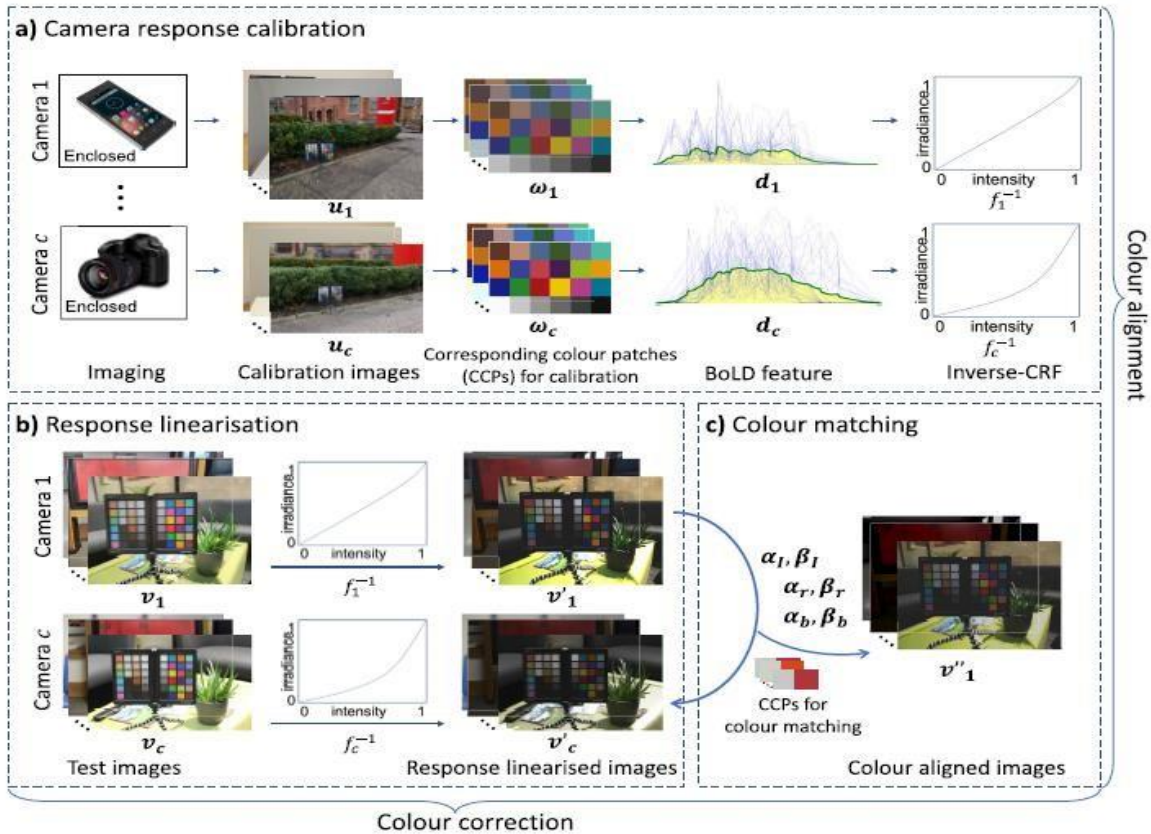


Fig-1: Three step color alignment framework

3.1 Color Alignment Framework

The test images captured by that camera are then color-linearized by applying the calibrated nonlinear camera response. In the final step, the intensity and chromaticity of the color-linearized images taken by different cameras are aligned to each other, producing the color-aligned images. where I represents the set of input images, $iCRF$ denotes the inverse camera response function, $L(iCRF(I))$ represents the color-linearized images obtained by applying $iCRF$ to the input images I , and $C(L(iCRF(I)))$ denotes the color-aligned images resulting from the color matching step applied to the linearized images. The objective is to find the optimal $iCRF$ that minimizes the color variations between color aligned images.

$$\arg \min_{\theta} \mathcal{J} \left(f_{\theta}^{-1} (u) \right)$$

$$v' = f_{\theta}^{-1} (v) = \begin{bmatrix} f_{\theta}^{-1} (D_1) \\ \vdots \\ f_{\theta}^{-1} (D_m) \end{bmatrix} \quad \text{Equation-1}$$

In the mathematical formulation, θ represents the optimal camera-dependent parameters to be calibrated, J denotes the color deviations between images and is calculated as shown by Eq. 16-20, and f_{θ}^{-1} is the parametric reconstruction of the inverse camera response function ($iCRF$) for a specific camera, where u and v are the calibration and test image vectors, respectively. To quantify the color deviations between images, a two-dimensional color constant pattern (CCP) vector needs to be constructed by extracting CCPs from the images. This CCP vector has the general form:

$$w = \begin{bmatrix} w_1 \\ \vdots \\ w_m \end{bmatrix} = \begin{bmatrix} p_1^1 & \dots & p_1^n \\ \vdots & \ddots & \vdots \\ p_m^1 & \dots & p_m^n \end{bmatrix} \quad \text{Equation-2}$$

In the formulation, w denotes the CCP vector collected from the calibration images. In the subsequent response linearization step, the images under examination are linearized in terms of color intensity, denoted as v' , by applying the optimal iCRF determined in the first step. This process is represented by Eq. 10. Linear transformation coefficients α and β are first estimated from the CCP vector w through a regression process by minimizing the color deviations between images, as shown in Eq. [X]. A minimum of two CCP's is required for this estimation, as two points determine a line.

$$\arg \min_{\alpha, \beta} = \mathcal{J} \left(\begin{bmatrix} \alpha_1 p_1^1 + \beta_1 & \dots & \alpha_1 p_1^n + \beta_1 \\ \vdots & \ddots & \vdots \\ \alpha_m p_m^1 + \beta_m & \dots & \alpha_m p_m^n + \beta_m \end{bmatrix} \right) \text{, Equation-3}$$

The linear transformation coefficients α and β , estimated through the regression process using the CCP vector w from the test images.

$$v'' = \alpha v' + \beta = \begin{bmatrix} \alpha_1 v'_1 + \beta_1 \\ \vdots \\ \alpha_m v'_m + \beta_m \end{bmatrix} \text{ Equation-4}$$

3.2 Camera response calibration

In this paper, camera response calibration is approached as the process of estimating the nonlinearity in color intensity. Two calibration approaches are proposed: 1) Selection of the optimal camera response function (CRF) from the database of response functions (DoRF) through exhaustive search. 2) Calculation of the optimal CRF model parameters by machine learning-based optimization. The Empirical Model of Response (EMoR) is used as the CRF representation model in the optimization approach. The intensity distance refers to the intensity offsets between color constant patterns (CCP's). The intensity distances calculated from RAW images taken by a digital camera (i.e., images with a linear CRF) are visualized in and it can be observed that they are nearly symmetric along the x-axis (i.e., with respect to the intensity of CCPs) when the applied CRF is linear.

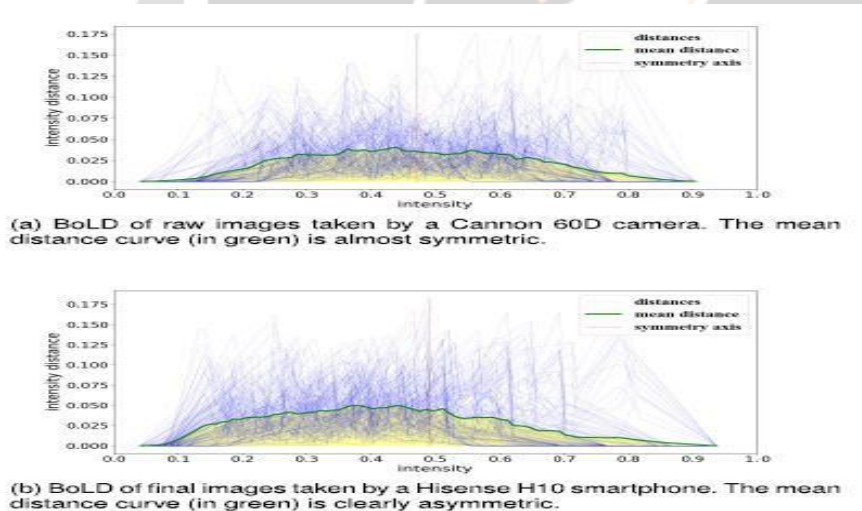


Fig-2: Visual explanation of the BLOD feature. 20 images were taken by each of these cameras. The images were taken under various uniform illuminations. 24 CCP's were extracted from each of these images. The CCP's were sorted based on their intensity values. The blue lines are rendered from the calculated d . The green curve was drawn from the mean intensity distance d . The area under the d curve is marked yellow. And the red dashed line denotes the symmetry axis of d .

To calculate the BOLD value, the color intensity values of the CCP's are first extracted from the images used for calibration and encapsulated in a two-dimensional CCP vector similar to Eq. 11. The rows of the vector represent different calibration images, while the columns represent the varying intensities of the CCP's. The columns of the CCP vector are sorted according to their mean values. Subsequently, the color intensity values in the CCP vector are converted into irradiance values and aligned with each other based on the first and last columns in the sorted CCP vector:

$$\arg \min_{\alpha, \beta} = \mathcal{J} \left(\begin{bmatrix} \alpha_1 p_1^1 + \beta_1 & \alpha_1 p_1^n + \beta_1 \\ \vdots & \vdots \\ \alpha_m p_m^1 + \beta_m & \alpha_m p_m^n + \beta_m \end{bmatrix} \right)$$

$$w'_u = \begin{bmatrix} \alpha_1 f_{\theta}^{-1}(p_1^1) + \beta_1 & \dots & \alpha_1 f_{\theta}^{-1}(p_1^n) + \beta_1 \\ \vdots & \ddots & \vdots \\ \alpha_m f_{\theta}^{-1}(p_m^1) + \beta_m & \dots & \alpha_m f_{\theta}^{-1}(p_m^n) + \beta_m \end{bmatrix}$$

Equation-5

This produces the color-aligned CCP vector w'_u . A two-dimensional mean CCP vector \bar{W} is then constructed by joining m one-dimensional mean CCP vectors \bar{w} , which are themselves calculated by averaging the color-aligned CCP's along the calibration images:

$$\bar{w} = \frac{\sum_{i=1}^m f_{\theta}^{-1}((w'_u)_i)}{m}$$

$$\bar{W} = \left[\begin{array}{c} \bar{w} \\ \vdots \\ \bar{w} \end{array} \right]_m$$

$$d = |w'_u - \bar{W}| \quad \bar{d} = \frac{\sum_{i=1}^m d_i}{m}$$

Equation-6

The CCP vector w'_u , which is aligned with the color, and the mean CCP vector \bar{W} are positioned between each other. The mean intensity distance curve is generated by calculating the average of d in the column direction. Ultimately, the BOLD value, represented as B , is determined through the l_2 -norm of the normalized asymmetry coefficient and the weighted area under the d curve:

$$B = \|\eta - \lambda_1 \phi, \lambda_2 \mu\|_2$$

$$\eta = \frac{\sum (x - \bar{x})^3}{s \left(\sum (x - \bar{x})^2 \right)^{\frac{3}{2}}}$$

$$\phi = \max(\bar{d}) + \min(\bar{d}) - 1$$

$$\mu = \sum \bar{d}$$

Equation-7

In the given context, the symbol μ represents the area under the d curve. The variables x and \bar{x} represent the uniformly sampled values on d and the mean of the samplings, respectively. The number of samplings, denoted as s , was determined through empirical selection and set to 100. To mitigate the impact of skewed samplings in the intensity.

Algorithm 1 Pixel-Wise Linear Colour Matching Algorithm

Input: *image1* is the image to be matched and *image2* is the image to be corrected;

Output: *image2*;

- 1: $R_1, G_1, B_1 \leftarrow R, G, B$ values of the CCPs in *image1*;
- 2: $R_2, G_2, B_2 \leftarrow R, G, B$ values of the CCPs in *image2*;
- 3: $I_1 \leftarrow R_1 + G_1 + B_1$;
- 4: $I_2 \leftarrow R_2 + G_2 + B_2$;
- 5: $\alpha_I, \beta_I \leftarrow$ linear regression on $\{I_1, I_2\}$;
- 6: $\alpha_r, \beta_r \leftarrow$ linear regression on $\left\{ \frac{R_1}{I_1}, \frac{R_2}{I_2} \right\}$;
- 7: $\alpha_b, \beta_b \leftarrow$ linear regression on $\left\{ \frac{B_1}{I_1}, \frac{B_2}{I_2} \right\}$;
- 8: *image2* $\leftarrow I_2$ scaled by α_I and offset by β_I ;
- 9: *image2* $\leftarrow \frac{R_2}{I_2}$ scaled by α_r and offset by β_r ;
- 10: *image2* $\leftarrow \frac{B_2}{I_2}$ scaled by α_b and offset by β_b ;
- 11: **return** *image2*;

to prevent the occurrence of discontinuous iCRF, in addition to the BOLD value. The CRF's in the DORF exhibit monotonicity, which implies that the iCRF is also monotonic. To minimize ambiguity, the monotonicity is included as a constraint in the cost function. The calculation of the optimal EMOR model parameters θ is then performed as:

$$\theta = \arg \min_{\theta} \left\| \mathcal{B}, \psi_1 \left| f_{\theta}^{-1''} \right|, \psi_2 \sqrt{\frac{\sum^M \left(f_{\theta}^{-1''} - \overline{f_{\theta}^{-1''}} \right)^2}{M}} \right\|_2^2$$

subject to $f_{\theta}^{-1'} > 0$

Equation-8

The micro-smoothness restriction, which is weighted by ψ_1 , ensures that there are no discontinuous iCRF's. Meanwhile, the macro-smoothness restriction, which is weighted by ψ_2 , preserves the overall shape of the iCRF. The number of homogeneous macro-samplings on the candidate iCRF, denoted as M and set to 10, plays a role in this process. Monotonicity is guaranteed by a positive first-derived iCRF. Ultimately, the Optimization approach reconstructs the iCRF based on the calculated EMOR.

$$f^{-1} = H_0^{-1} + \theta^T H_{1:k}^{-1}$$

The mean and first k eigenvectors of all iCRF's in the DORF are denoted as $H^{-1} 0:k$.

Pixel-Wise Linear Colour Intensity and Chromaticity Matchings

After calibrating the optimal iCRF, images captured with the identical camera can be converted into a linear response space through interpolation based on the estimated iCRF outlined in Equation 10. Upon completion of linearization, the color intensity and chromaticity of any pair of such images are aligned linearly.

Algorithm 2 Pixel-Wise Independent Colour Modification Algorithm

Input: *image1* is the image to be independently colour intensity and RB chromaticity modified. α_I and β_I are the colour intensity scaling and offset coefficients. α_r and α_b are the scaling coefficients for red and blue chromaticity, respectively. β_r and β_b are the offset coefficients for red and blue chromaticity, respectively;

Output: *image2*;

- 1: $R', G', B' \leftarrow R, G, B$ pixel values in *image1*;
- 2: $R' \leftarrow \alpha_I R'$;
- 3: $G' \leftarrow \alpha_I G'$;
- 4: $B' \leftarrow \alpha_I B'$;
- 5: $R \leftarrow \frac{(R'+G'+B'+\beta_I)R'}{R'+G'+B'}$;
- 6: $B \leftarrow \frac{(R'+G'+B'+\beta_I)B'}{R'+G'+B'}$;
- 7: $G \leftarrow R' + G' + B' + \beta_I - R - B$;
- 8: $R' \leftarrow \alpha_r R$;
- 9: $B' \leftarrow \alpha_b B$;
- 10: $G' \leftarrow R + G + B - \alpha_r R - \alpha_b B$;
- 11: $R \leftarrow \beta_r (R' + G' + B') + R'$;
- 12: $B \leftarrow \beta_b (R' + G' + B') + B'$;
- 13: $G \leftarrow R' + G' + B' - R - B$;
- 14: *image2* $\leftarrow R, G, B$;
- 15: **return** *image2*;

Algorithm 2 summarizes the process of independently modifying the color intensity and chromaticity without impacting the other component. Unlike the previous sections, where the modifications were in general forms, this algorithm provides specific instructions for intensity and chromaticity adjustments.

RESULTS:

The image utilized as an input for image processing in a MATLAB program was captured using a smartphone camera. The primary goal of this endeavor is to develop a proficient color constancy method for images.

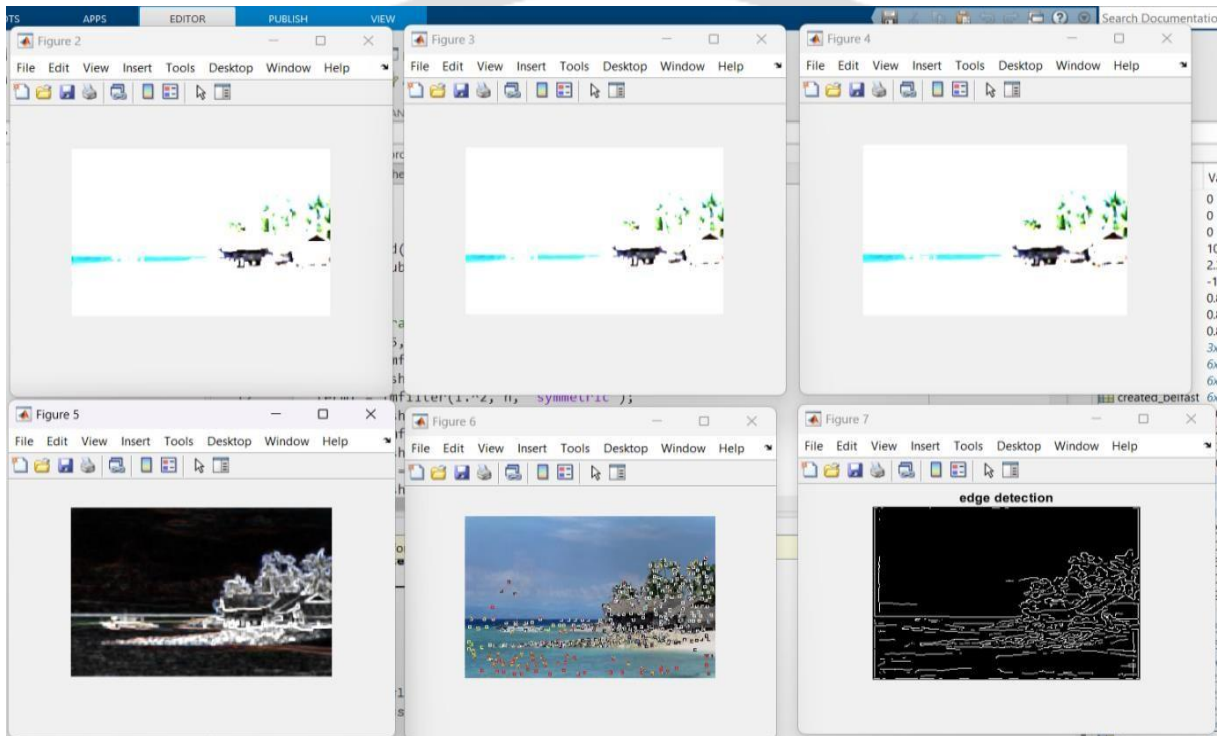


Fig 3.Input image



Fig10. Output image

During the process of color constancy, the identification of edges and CRF within the image is carried out, followed by the analysis of color variations present in the image



The CRF images, denoted as Figure [4,5,6], depict the camera response frame. On the other hand, Figure [7,8,9] showcases the images related to edge detection and color patch detection.

Evaluation Metrics:

The RMSE, RAE, and 1E 2000 are commonly used metrics for evaluating color differences. The RMSE is particularly suitable for assessing differences in color intensity by calculating the Euclidean distance between two compared colors. However, the RMSE is not as effective in measuring chromaticity differences, as chromaticity is the ratio of a color channel to its intensity. On the other hand, the RAE quantifies the angular disparity between two colors or pixels as directed vectors, making it a reliable metric for estimating chromaticity differences that are not influenced by color intensity. Lastly, the 1E 2000 metric is employed to measure color differences based on visual perception.

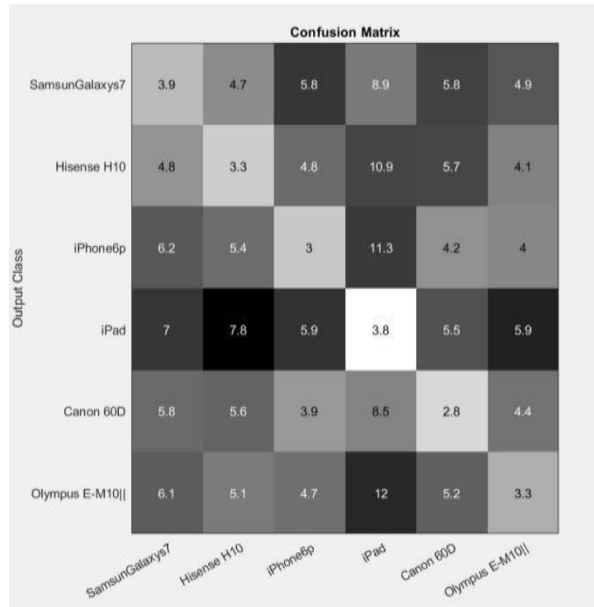


Fig.10. Heat map visualisation of the single and cross camera RCC performance on the Belfast (left), modified Middlebury (middle), and rendered Gehler-Shi , (right) datasets. The BoLD-alignment performance was measured by 1E 2000.

A. The Overall RCC Performance

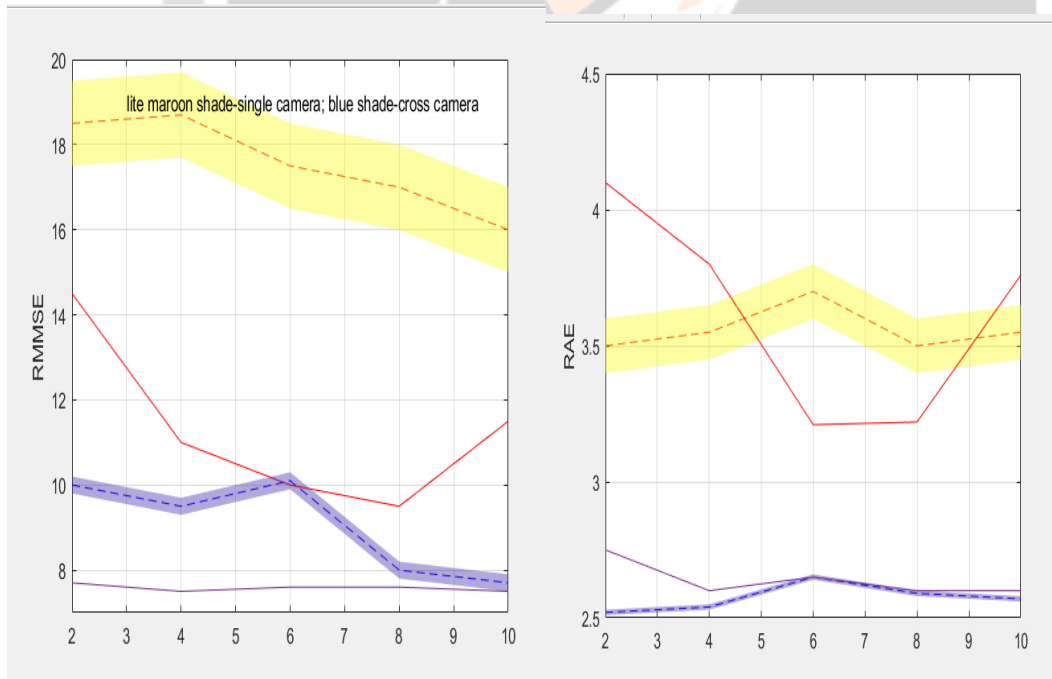


Chart-1 Number of calibration images

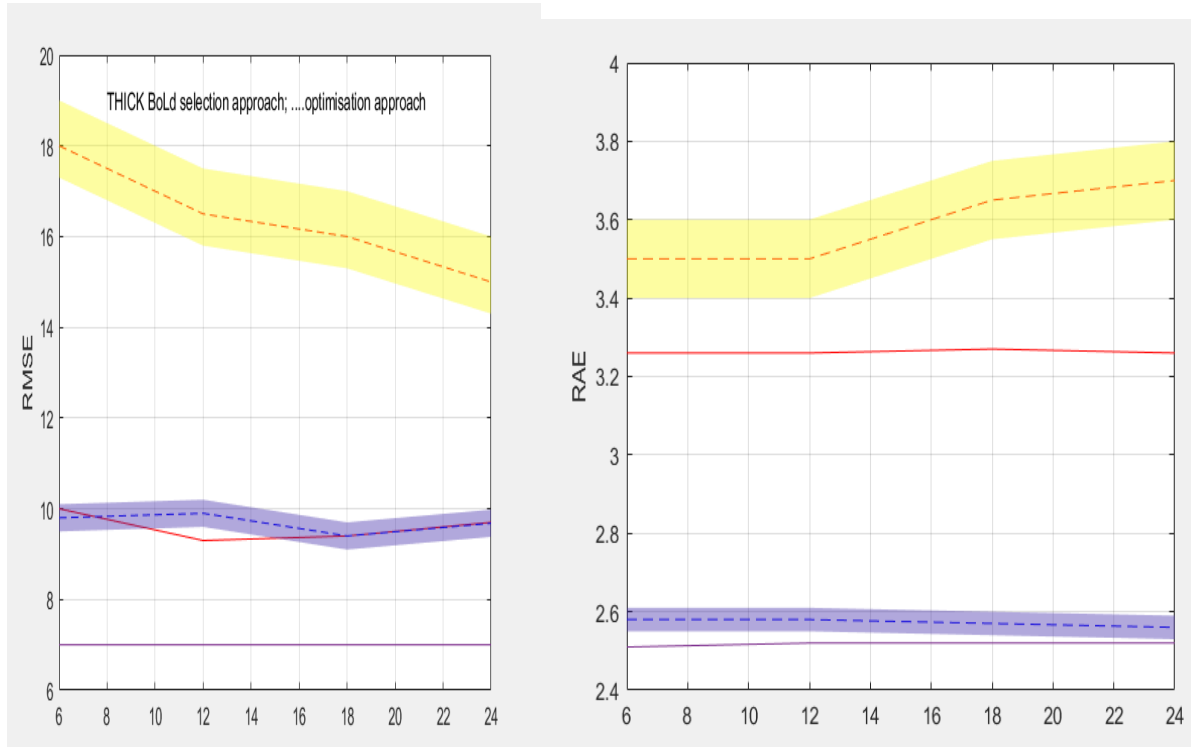


Chart-2 Number of Corresponding Color patches for Calibration

■ Single camera ■ Cross camera -- Bold selection approach -- optimisation approach.

Single (blue curves) and cross (orange curves) RCC performance of the Optimisation (dashed curves) and Selection (solid curves) calibration approaches with applying different NoCIs (2, 4, 6, 8, and 10) and NoCCP- CAs (6, 12, and 24). The grey area indicates the standard derivation (SD, n = 3) by the Optimisation approach.

The minimum number of calibration images (NoCI) required for the proposed calibration is an important consideration. It is desirable for the user to prepare as few calibration images as possible while still achieving accurate results. The results shown in Figure 6 were obtained using both the Optimisation and Selection calibration approaches, with different NoCIs (2, 4, 6, 8, and 10), while keeping NoCCP-CA fixed at 12 and NoCCP-CM fixed at 24. These results indicate that the Selection approach outperformed the Optimisation approach in terms of the root mean square error (RMSE) for both single and cross camera relative color correction (RCC) performance. Additionally, the RMSE values produced by the Selection approach were closer to each other compared to those produced by the Optimisation approach. The relative absolute error (RAE) performance did not show significant differences between the Selection and Optimisation approaches, nor between the single and cross camera RCC performance. Generally, a larger NoCI improved the overall camera color calibration performance in terms of RMSE, but had no effect on the performance in terms of RAE.

B. Model Parameter

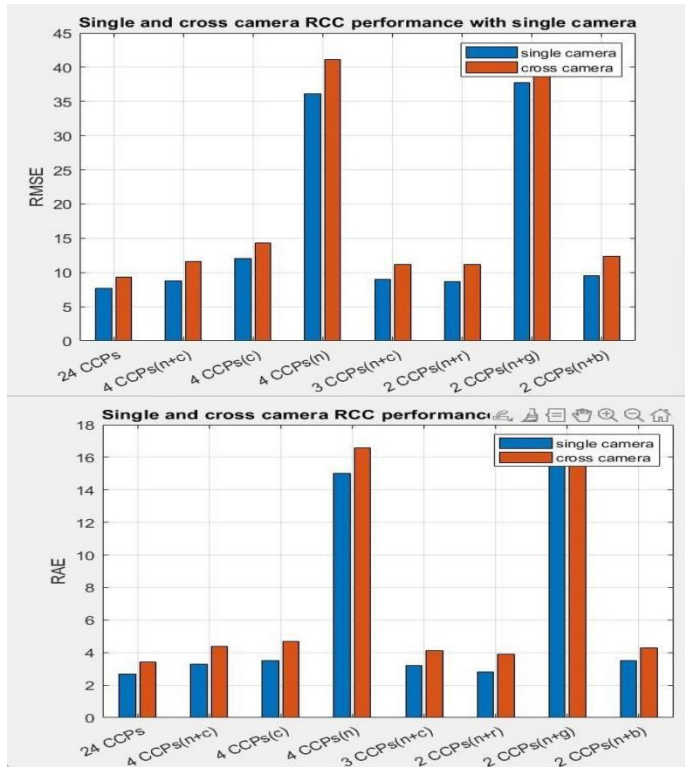
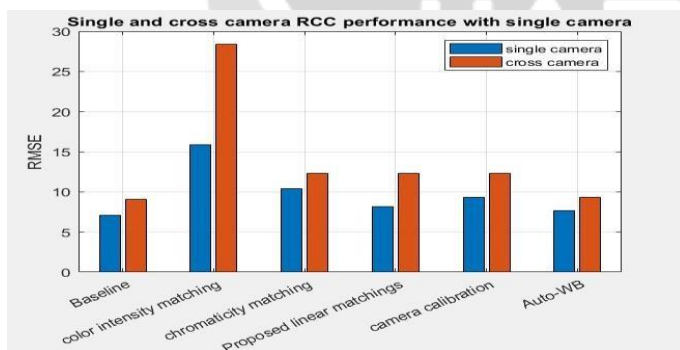


Chart-3 Single and cross camera RCC performance in terms of the RMSE and RAE using different number and composition of CCP's for colour matching. In this figure, n stands for neutral, c represents colorful such as red (r), green (g), and blue (b) CCP's. Color matching using all the color patches on a Macbeth chart (24 CCP's) was the comparison baseline. The CCPs used for each matching are indicated on top of the diagram where each colored square represents an applied CCP.



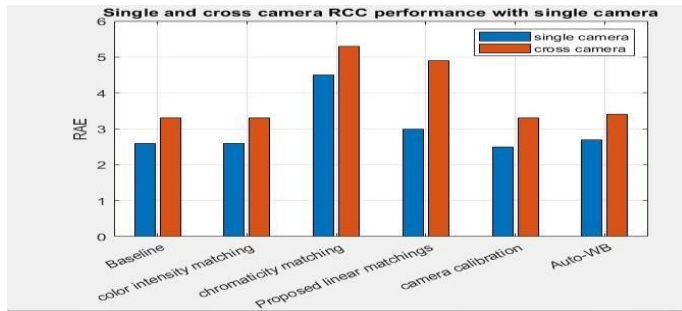


Chart-4.Single (blue bars) and cross (orange bars, i.e., color alignment between images taken by different cameras) camera RCC performance contributions in terms of the RMSE and RAE of the different components in the BoLD-alignment are evaluated, compared and discussed in the text.

1) The experiment focused on analyzing the impact and effectiveness of different numbers of Corresponding Colour Patches for Colour Matching (NoCCP-CM) and the selection of which patches to use. The study utilized the BoLD-alignment method and varied the number and composition of CCP’s for color matching, while keeping the number of independent colorants (NoCI) fixed at eight and the number of Corresponding Colour Patches for Color Appearance (NoCCP-CA) fixed at 24. The comparison baseline was set by using all the color patches on a Macbeth chart as CCP’s, which was assumed to provide the best possible performance.

The results, as depicted in Figure 7, showed that using a larger number of NoCCP-CM generally resulted in higher performance in terms of Relative Colorimetric Consistency (RCC). However, since obtaining CCP’s can be costly, there needs to be a balance between the number of CCP’s and the RCC performance. Based on the experimental findings, using a combination of two mixed-color CCP’s ($n = 2$) is the optimal choice when there is a limitation on the number of CCP’s for color matching. This option still provides satisfactory performance, although it heavily relies on the selection of CCP color composition. On the other hand, using 24 Macbeth CCP’s ($n \geq 4$) is preferable when prioritizing algorithm performance and stability.

The performance of color matching is greatly influenced by the careful selection of CCP’s. When examining two mixed-color CCP’s that utilized red, green, and blue as the colorful CCP, the performance achieved with a red or blue CCP was satisfactory but unsatisfactory compared to that achieved with a green CCP. This is attributed to the high BR chromaticity ratios (Eq. 28) for the red (2.90) and blue (2.67) CCP’s and the low ratio in the case of a green (1.27) CCP. This suggests that CCP’s with higher BR chromaticity ratios result in better correction accuracy. The comparison of various compositions of CCP’s (neutral or colorful patches only and mixed patches) in Fig. 7 demonstrated that a combination of neutral and colorful CCP’s enhanced the RCC performance. This is because they offer a wider range of color intensity and chromaticity coverage. These conclusions regarding CCP selection also hold true for CCPs used in camera calibration.

TABLE I

SINGLE AND CROSS CAMERA RCC PERFORMANCE BENCHMARK EVALUATED IN TERMS OF THE RMSE (IN INTENSITY), RAE (IN DEGREE),AND 1E 2000 USING THE THREE IMAGE DATASETS. OUR BOLD-ALIGNMENT ACHIEVED THE BEST PERFORMANCE

```

MATLAB R2013b
HOME PLOTS APPS
New Script New Open Find Files Import Save Open Variable Analyze Code Preferences Community
Compare Workspace Clear Workspace Run and Time Simulink Layout Set Path Help Request Support
Add-Ons
FILE VARIABLE CODE SIMULINK ENVIRONMENT RESOURCES
E:\matlab\dip\dip\23\Color_Alignment_for_Relative_Color_Constancy_via_Non_Standard_References\code
Command Window
New to MATLAB? Watch this Video, see Examples, or read Getting Started.
created_belfast =

    proposed_parameter    value
    _____    _____

    'RMSE_single'        10.74
    'RMSE_cross'         15.41
    'RAE_single'          2.77
    'RAE_cross'           3.91
    'DELTAe200_single'    4.01
    'DELTAe200_cross'    5.23
    
```

Table I displays the results of the benchmark, which compares the proposed BoLD-alignment with other popular and state-of-the-art methods in terms of the RMSE, RAE, and 1E 2000 metrics. The best performance for each metric is highlighted in bold. In comparison, our method, utilizing either two (Colour patch number 1 and 9) or three (Colour patch number 1, 9, and 11 on the Macbeth chart) NoCCP-CMs, achieved the highest overall RCC performance across the three datasets. This was particularly evident in the modified Middlebury dataset, which simulates uncommon scientific imaging scenes. Our method outperformed both the tested statistical and learning-based WB methods that solely considered illuminations. Furthermore, it demonstrated superior performance compared to colour matching methods that employed identical or larger NoCCP-CMs.

TABLE II

```

MATLAB R2013b
HOME PLOTS APPS
New Script New Open Find Files Import Save Open Variable Analyze Code Preferences Community
Compare Workspace Clear Workspace Run and Time Simulink Layout Set Path Help Request Support
Add-Ons
FILE VARIABLE CODE SIMULINK ENVIRONMENT RESOURCES
E:\matlab\dip\dip\23\Color_Alignment_for_Relative_Color_Constancy_via_Non_Standard_References\code
Command Window
New to MATLAB? Watch this Video, see Examples, or read Getting Started.
modified_middle_bury =

    proposed_parameter2    value2
    _____    _____

    'RMSE_single'        12.38
    'RMSE_cross'         17.52
    'RAE_single'          2.41
    'RAE_cross'           4.58
    'DELTAe200_single'    3.89
    'DELTAe200_cross'    5.59
    
```

The computation time benchmark for calibration and correction involved comparing the time required to calibrate each camera and correct an image. The results of this benchmark are presented in Table II. The Reference and Exposure camera response calibration approaches were utilized for comparison purposes. In the Reference approach, a polynomial regression ($d = 6$) on the standard reference values was completed within 0.005s. This process was exceptionally fast thanks to the well-optimized and relatively simple implementation of the polynomial regression code. On the other hand, the Exposure calibration approach involved

calculating the optimal iCRF using pre-set exposure times and machine learning-based optimization. In contrast to the swift Reference approach, the Exposure approach took 165.77s to complete. For our proposed camera response calibration, the Selection approach only required 3.50s to complete the task, while the Optimisation approach took 1812.33s. In the subsequent section, it is evident that our method (0.92s) operated slightly slower than the statistical-based WB methods due to the nonlinear interpolation during response linearization, yet it was faster than the learning-based method.

4. CONCLUSION

The paper introduces a high-performance color alignment model designed to align the colors of images captured by different cameras under various lighting conditions. The model comprises three main steps: camera response calibration, response linearization, and color matching. The first step is a one-time process for each device and is suitable for commercial digital cameras that do not provide access to internal imaging sensor data. Standard color references are not necessary. The second step is faster than neural network-based methods and can be used on portable devices like smartphones. In the third step, only two CCPs are required for color matching, making it more cost-effective for consumer-oriented imaging applications. Overall, our model has demonstrated superior RCC performance on image datasets.

5. REFERENCES

- [1] Yunfeng Zhao , Stuart Ferguson , Huiyu Zhou , Christopher Elliott , and Karen Rafferty “Color Alignment for Relative Color Constancy via Non-Standard References” IEEE TRANSACTIONS ON IMAGE PROCESSING, VOL. 31, 2022.
- [2] I. Hussain and A. K. Bowden, “Smartphone-based optical spectroscopic platforms for biomedical applications: A review [invited],” *Biomed. Opt. Exp.*, vol. 12, no. 4, pp. 1974–1998, Apr. 2021.
- [3] S. Banik et al., “Recent trends in smartphone-based detection for biomedical applications: A review,” *Anal. Bioanal. Chem.*, vol. 413, no. 9, pp. 2389–2406, 2021.
- [4] X. Huang et al., “Smartphone-based analytical biosensors,” *Analyst*, vol. 143, no. 22, pp. 5339–5351, Oct. 2018.